Xu *et al. Heritage Science* (2023) 11:250
https://doi.org/10.1186/s40494-023-01095-z

Heritage Science

COMMENT

Open Access

The effects of construction vibration on stone cultural relics: a case study from the Qingdao Museum

Weixiao Xu[1*], Jixing Zhao[1], Weisong Yang[1], Dehu Yu[2], Lingling Qiu[2], Zhenlong Chen[3] and Yusheng Qiu[4]

Abstract

The potential impact of vibration from nearby construction on four ancient stone statues in the Qingdao Museum was studied. Simulated but full-scale drilling, excavation and impact breaking were conducted to gather ground motion data which were used to prepare incremental dynamic time histories. The four stone statues were modeled numerically and the models were used to estimate the statues' maximum tensile stress, maximum strain and maximum shear stress in response to the time histories. The most vulnerable parts of the statue are thus identified, and vibration limits were proposed.

Keywords Construction vibration, Statues, Vibration limits, Time history analysis

Introduction

Common construction activities such as driving impact piles, blasting and digging can induce substantial ground vibrations which can have an adverse effect on the surrounding environment. Beyond disrupting the normal work and life of nearby residents and workers, such construction-related vibration can actually damage precision instruments and cultural relics [1–4]. Precision instruments often have well-defined allowable vibration thresholds [5–9]. Cultural relics, however, vary greatly in composition, age, weight and volume, which makes specifying standard allowable vibration limits difficult [10–12].

Capsule boxes and exhibition cases are effective means of safeguarding smaller and lighter cultural artifacts against construction-induced vibrations. However, larger stone sculptures, due to their substantial size and direct contact with the floor or ground, are more vulnerable to such vibrations.

Numerous academics have conducted research on the impact of vibrations originating from various sources on significant cultural artifacts, architectural structures, and artistic masterpieces. A group led by De Stefano prepared a numerical simulation of the Holy Shroud Chapel in Turin and stressed it with vibration monitored in field tests, including vibration from hammering, heavy falling objects and wind vortices generated by passing helicopters [13]. Johnson and his colleagues studied the vibration thresholds and vibration control techniques under various conditions in connection with the reconstruction and expansion projects of the Chicago Academy of Arts and the St. Louis Museum of Art. The concern was about the possibility of damage to various important cultural relics and works of art. After monitoring the vibration resulting from site preparation, excavation, demolition and pile installation, the maximum velocity peak in each phase of the work was obtained. The authors then proposed a

*Correspondence:
Weixiao Xu
wxgodspeed@163.com
[1] College of Civil Engineering, Qingdao University of Technology, Qingdao 266033, China
[2] College of Civil Engineering, Shandong Jianzhu University, Jinan 250101, China
[3] Qingdao Zhongjian Combination Group Co. Ltd., Qingdao 266061, China
[4] The Qingdao Museum, Qingdao 266061, China

five-stage vibration control technique which they applied successfully in both projects [14]. In order to protect the dinosaur fossils from the Philadelphia Museum being exhibited in Chicago, the same group later formulated structural damping measures to protect them based on the vibration excitations they collected under six different conditions that could have been encountered during the exhibition. Their studies showed that the measures greatly weakened the influence of environmental vibration on the fossils [15].

The Okumus group has studied the influence of vibration from the pouring of three reinforced concrete columns on a surrounding operating room and animal laboratory [16]. Their work showed that the vibration generated by general construction activities was within vibration limits allowed for operating rooms by the specifications of the International Standards Organization, but the low-frequency vibration generated by the pouring of the columns in the basement exceeded the operating room limit. A group led by Zini analyzed the influence of road traffic vibration on an ancient stone lodge and compared it with vibration monitoring observations. The results showed that uneven road surface and heavy traffic were the main reasons for an observed increase in building vibration [17].

Pieraccini and his colleagues summarize the results of a 2-day dynamic monitoring of Michelangelo's David subject to environmental loads (city traffic and pedestrian loading induced by tourists visiting the Accademia Gallery) [18]. To evaluate the effects of the pedestrian loading induced by visitors, the radar measure-ments were taken on a closing day of the museum, and repeated on the second opening day (statistically the day with higher tourist affluence). A numerical model of the statue was employed to evaluate the experimental results. The presence of the audience has affected only the lower resonance frequency, thus increasing the average amplitude of the displacement of about 60%. Despite this increase, the absolute value of the average displacement amplitude remains small.

Siami and his colleagues are dedicated to present some methods for vibration protection of statues and cultural heritage objects against earthquakes and ambient vibrations [19]. They open with short explanation about the dynamic performance test that has been done on a full-scale copy of the famous statue of Michelangelo Buonarroti Pieta Rondanini and its isolation system. Based on the results of the tests, a multidegree-of-freedom model is developed. This updated model is used to verify the proposed vibration control strategies. To reduce the level of vibration transmitted to the statue, combination of inerter with TMD (TMDI) is proposed. Optimal parameters of the passive device are found by using numerical methods. Furthermore, a scaled isolation system is designed and manufactured according to the test results of the full-scale structure. To improve the performance of the isolator, a designed and manufactured ball-screw type inerter is introduced to the scaled structure. The effectiveness of the manufactured inerter on the dynamic behavior of the isolation system is demonstrated by using dynamic performance tests on a shaking table. The results provide some numerical and experimental results considering inerter-based methods in order to vibration protection of statues and cultural heritage.

From China, Dai and his colleagues report [20] carrying out real-time vibration monitoring of the Hunan Provincial Museum during construction of the shield for Changsha's Metro Line 6. Their study showed that the vibration caused by the shield construction could be effectively reduced by modifying the construction parameters, adjusting the tunnel's axis and damping the horizontal transportation system. The aforementioned procedures have effectively ensured the safety of the museum and its cultural artifacts.

In summary, an increasing number of scholars are paying attention to the influence of construction vibration on historical buildings, museums and museum collections. This study had four stone statues exhibited in the Qingdao Museum as its relics of concern. Ground motion data were used to quantify an incremental dynamic time-history analysis predicting the statues' dynamic responses to vibration, including the maximum tensile stress, maximum strain and maximum shear stress. The vulnerable parts of the statues were identified, offering a point of reference for safeguarding them against potential damage caused by construction-induced vibrations.

Research object

The Qingdao Museum is classified as a prestigious national museum in China. It displays paintings, calligraphy and cultural relics from the Neolithic age to the Ming and Qing dynasties and modern times. However, the building's floor area is only 25,000 square metres, which is insufficient for the volume of tourists. Consequently, plans have been made to expand the museum.

Two stone statues of the Buddha dating from the Northern Wei Dynasty and two stone Bodhisattva statues from the Northern Qi Dynasty (see Fig. 1) are displayed on the first floor of the museum, the construction of stone sculptures dates back over 1400 years ago. They are among its most precious cultural relics. The two stone Buddha statues are carved from limestone. They each stand 5.8 m tall and weigh about 30 tonnes. They stand directly on the buildings foundations to bear the weight. The other two statues (Fig. 2) are Mahastamaprapta and Kwanyin bodhisattvas, also of limestone

Fig. 1 Stone Buddha statues

Fig. 2 Bodhisattva statues

and approximately 3.46 m tall. They are supported by the building's first story. The four statues cannot be transferred to other safe locations during the expansion project due to their size and field conditions.

Vibration testing

Before construction began, vibration tests were conducted which simulated the vibration expected during different construction activities, and the relics' realistic vibration characteristics were recorded. The vibration velocity–time history signals for each construction activity obtained through the testing were used to quantify numerical models of the four statues for further study.

Instrumentation

The vibration sensors used in the tests were 941B ultralow-frequency sensors with a pickup sensitivity of 23 V·s/m and a maximum range of 0.125 m/s. The SCADAS general dynamic data acquisition instrument

Fig. 3 Position of the vibration picker at the test point

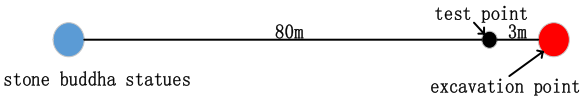

Fig. 4 Vibration test arrangement

produced by the LMS company in Denmark was used. It offers 200 Hz sampling rate. According to the requirements of the Technical Specification for the Prevention of Industrial Vibration of Ancient Buildings, the uniform sampling time is 15 min.

An excavation point was selected 80 m away from the cultural relics, and the lateral and vertical velocity–time history of the vibrations was recorded at a position 3 m away from the excavation point, as shown in Figs. 3 and 4.

Test conditions

The three construction processes tested were drilling (hammer penetration with a heavy-duty power contact machine, hammer weight 63.5 kg, drop distance 76 cm, hammering rate 15–30 blows per minute), excavation and impact breaking (with a 175 mm hammer) (see Fig. 5). The resulting signals were designated as time history 1 for the drilling, time history 2 for the excavation and time history 3 for the impact breaking. The signals generated by excavation and impact breaking reflected both the vibration generated by the excavator on the surface and that from the strong rock layer under the surface.

Test results

The frequency domain signals obtained after fast Fourier transform of each time domain signal are shown in Figs. 6, 7 and 8. In this discussion, X is the east–west direction, Y is north–south direction, and Z is the vertical direction.

Fig. 5 Construction site of each working condition

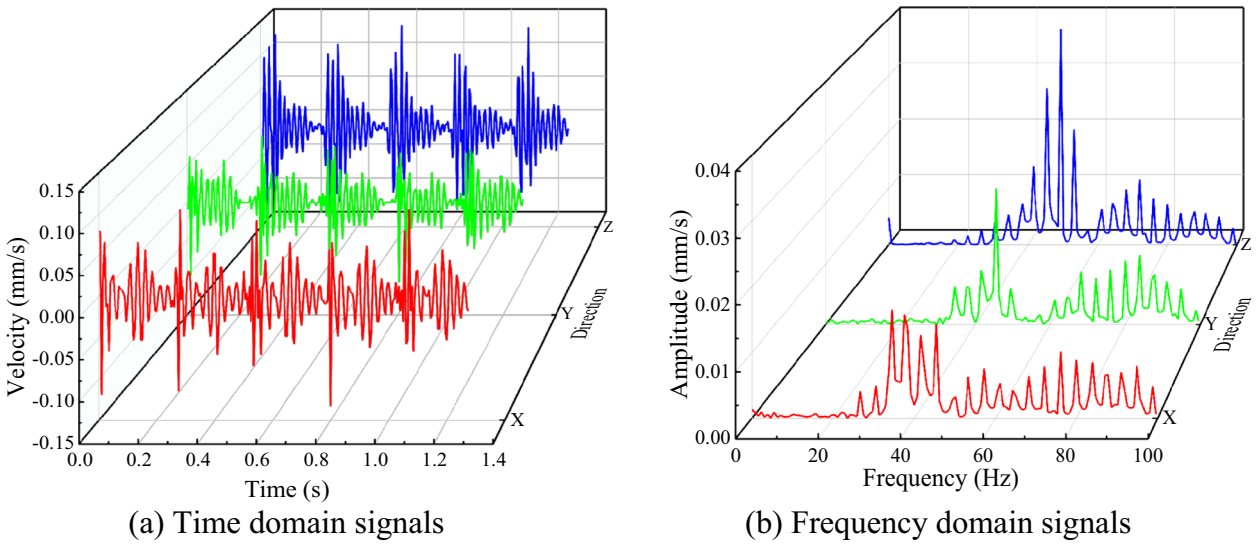

Fig. 6 Time history 1 three-dimensional time domain and frequency domain signals

Numerical simulation

Modeling method

The researchers employed three-dimensional laser scanning techniques to acquire three-dimensional point clouds that accurately depict the characteristics of the four relics. Digital image shell models were then generated using 3D Studio Max software. Subsequently, Hypermesh software was used for pre-processing the models and applying a mesh, which completes the statue of the model entity 1:1 model. Considering the complexity and calculation time involved, the tetrahedral mesh was selected. The maximum mesh size was controlled to below 0.05 m. Consequently, the model consists of a substantial number of unit nodes, specifically 1.4×10^5 units for the two stone Buddha statues and 1.5×10^5 units for the two bodhisattva statues. The partitioned models are shown in Figs. 9, 10, 11 and 12.

The three-dimensional velocity time history signals of the three construction processes were then used as excitation. Uniform excitation was applied to the bottom level of the image at the same time. Newmark's direct integration method was used in the calculations.

Principles for judging damage to statues

The article is based on the following three principles to determine whether the statue is damaged [21]:

1. Strain is the most direct evidence to reflect the deformation of the rock body and judge whether the rock

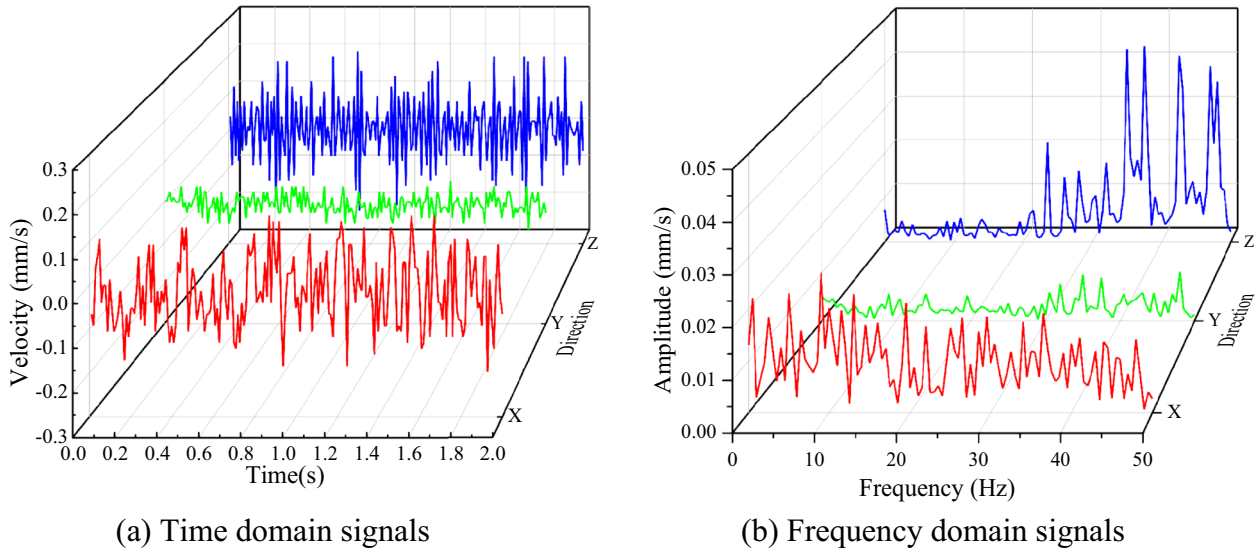

Fig. 7 Time history 2 three-dimensional time domain and frequency domain signals

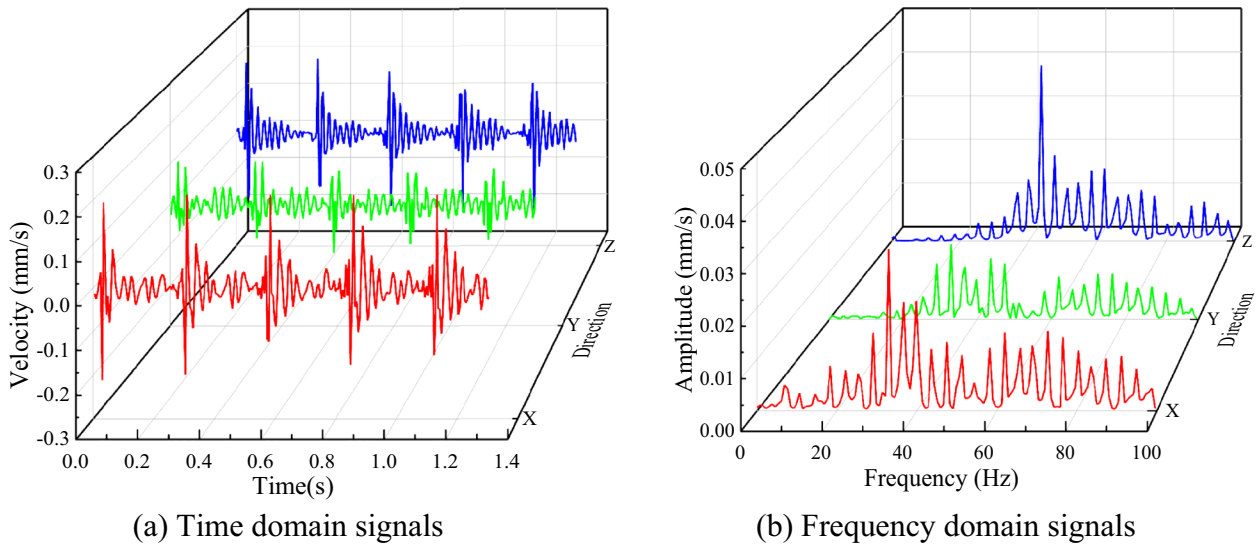

Fig. 8 Time history 3 three-dimensional time domain and frequency domain signals

body is damaged. Comparing the maximum strain values output from the three working conditions with the maximum critical strain values of similar greywacke in the references, it examines whether the statue will be deformed and damaged.

2. Unidirectional tensile damage occurs if the tensile stress on the rock body exceeds its tensile strength. When there are cracks in the rock body, due to the non-tensile property of the structural surface, it is most likely to pull apart along this set of cracks. By comparing the maximum tensile stress value of the statue with the tensile strength of the material, we can judge whether the statue will be tensile damaged.
3. According to Moore-Cullen strength theory, for brittle rock, when shear damage occurs at any point, the shear stress on the damage surface must be greater than the critical shear stress (the critical shear stress is equal to the sum of the material cohesion and the internal frictional resistance caused by the normal stress on the shear surface), so as to judge whether the statue will be damaged in shear.

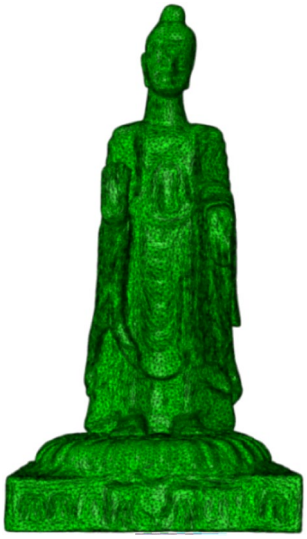

Fig. 9 Left Buddha statue model

Fig. 11 Mahastamaprapta status model

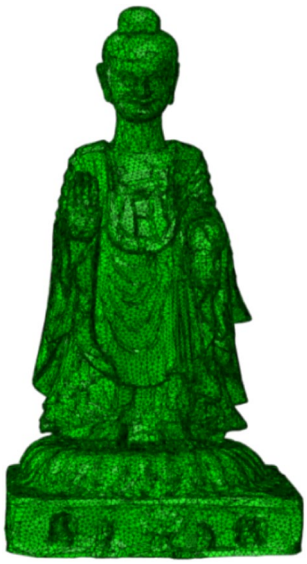

Fig. 10 Right Buddha statue model

Fig. 12 Kwanyin Bodhisattva statue model

Mechanical parameters of the materials

All four statues are known to have been carved from limestone excavated from the Longmen Grottoes. The mechanical parameters of Longmen Grottoes limestone are shown in Table 1 [21], and that density and Poisson's ratio were used in the modeling.

Since the elastic modulus is an important determinant of rock damage, the elastic wave velocity in the four statues was measured, and the elastic modulus was corrected based on the historical experience of the four statues, their internal and external cracks, any repair traces and the differences from the environment of the Longmen Grottoes.

Research has shown [22] that if rock is modeled as a Hooke medium, there is a certain correspondence between the propagation of acoustic waves in the rock and its mechanical properties. The relationship can be expressedas

Table 1 Mechanical parameters of Longmen Grottoes limestone

Elastic modulus (MPa)	Poisso's ratio	Density (g cm^{-3})	Compressive strength (MPa)	Tensile strength (MPa)	Cohesion (MPa)	Angle of internal friction
2.4×10^4	0.25	2.65	123	5.85	53	29°

Table 2 Relationship between rock wave velocity and weathering degree and the proportions of different degrees of weathering

	Degree of rock weathering			
	Unweathered	Slightly weathered	Moderately weathered	Strongly weathered
Rock wave velocity (km/s)	2.09–2.33	1.86–2.93	1.40–1.86	< 14.0
Left Buddha	6.67%	6.67%	33.3%	53.3%
Right Buddha	36.7%	4.55%	40.9%	18.2%
Mahastamaprapta	46.2%	0	15.4%	38.5%
Kwanyin Bodhisattva	33.3%	29.6%	11.1%	25.9%

$$u = \sqrt{\frac{E(1-\gamma)}{\rho(1-\gamma)(1-2\gamma)}} \quad (1)$$

where E is the elastic modulus; u is the acoustic velocity; ρ is the rock'sdensity; and γ is Poisson's ratio. Thus

$$E = \frac{u^2\rho(1+\gamma)(1-2\gamma)}{(1-\gamma)} \quad (2)$$

In this work ρ was taken as = 2650 kg/m^3 and γ as 0.25 (Table 1).

A location on one of the statues with relatively intact rock with only occasional weathering cracks was selected for testing the elastic wave velocity of 2326 m/s predicted by Eq. (1). The elastic wave velocities were then measured at several points on the four statues with various degrees of weathering to generate the weathering ratios shown in Table 2.

The weighted elastic modulus of each state was then calculated using Eq. (2) and the proportion of each degree of weathering. Considering that the statues' deformations must be controlled to within the elastic range, the four statues were regarded as ideal linear elastic bodies and the assumptions of classic elasticity theory were applied. A modified Mohr–Coulomb elastic–plastic model was used to simulate the limestone material under vibration [23]. The yield function of the constitutive model can reflect the isotropic hardening or softening of rock, as shown in Fig. 13 [24].

Since the modified Mohr–Coulomb constitutive model is an ideal linear elastic–plastic model, the absolute value of plastic strain is zero. Kong's group has studied the constitutive relationships of geomaterials and found [25] that

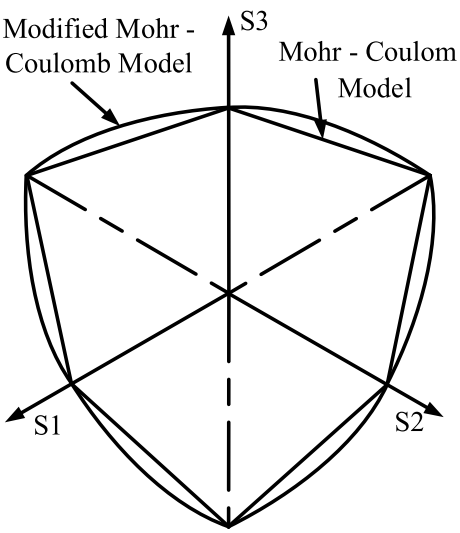

Fig. 13 The flow potential of the modified Mohr–Coulomb model

the dilatancy angle of geomaterials ψ can be taken as half of the internal friction angle. This was the relationship assumed for each statue.

The models' other material parameters used to estimate the parameters shown in Table 3 were taken from a geological survey report on the project site (Table 4).

Modal analysis and verification

Its vibration modes are an inherent and integral characteristic of an elastic structure. The first three natural frequencies of each stone statue calculated using mode analysis are shown in Table 5. The first-order frequency of stone Buddha statues was determined to be

Table 3 Mechanical parameters of each statue

Statue	Elastic modulus (GPa)	Poisson's ratio	Density ($g \cdot cm^{-3}$)	Internal friction angle (°)	Dilation angle (°)	Internal cohesion (MPa)	Absolute plastic strain
Left Buddha	5.70	0.25	2.65	29	14.5	53	0
Right Buddha	10.2	0.25	2.65	29	14.5	53	0
Mahastamaprapta	7.98	0.25	2.65	29	14.5	53	0
Kwanyin Bodhisattva	5.51	0.25	2.65	29	14.5	53	0

Table 4 Natural vibration frequencies of the statues

Left Buddha	Order	1	2	3
	Frequency (Hz)	11.2	19.0	42.1
Right Buddha	Order	1	2	3
	Frequency (Hz)	11.0	22.8	47.9
Mahastamaprapta	Order	1	2	3
	Frequency (Hz)	15.3	23.3	68.1
Kwanyin Bodhisattva	Order	1	2	3
	Frequency (Hz)	15.7	21.3	66.4

Table 5 Comparison of vibrational frequencies between the model and the measured vibration pattern of the stone statue

Model	Left Buddha	Order	1	2	3
		Frequency (Hz)	11.2	19.0	42.1
	Right Buddha	Order	1	2	3
		Frequency (Hz)	11.0	22.8	47.9
Actual	Left Buddha	Order	1	2	3
		Frequency (Hz)	12.5	17.9	48.6
	Right Buddha	Order	1	2	3
		Frequency (Hz)	12.1	19.4	48.9

approximately 11 Hz, with the second- and third-order frequencies approximately 19 and 48 Hz. The first-order frequency of the Bodhisattva statues is approximately 15 Hz, and the second- and third-order frequencies are approximately 21 and 68 Hz. Figure 14 shows the first three modes of the left Buddha statue and Fig. 15 shows them for the Mahastamaprapta statue. The first-order vibration mode of all four statues is in-plane inverted triangle vibration, and the second-order vibration mode is vertical vibration. That conforms to the vibration law, which supports the accuracy of the modeling. The natural frequencies of each order of each state are above 10 Hz, making them close to the high-frequency excitation frequency components generated by construction disturbance. Therefore, the influence of construction disturbance on the vibration of such stone statues cannot be ignored.

After a ten-minute environmental stimulation on the stone-caved Buddha statues, the obtained data is subjected to Fourier transformation for the extraction of the fundamental vibration frequencies, which are then compared with the results obtained from the finite element model to validate the accuracy of the model. Considering the large size and weight of the stone statues and their smooth surfaces, the testing sensors can only be positioned on the base of the statues, as illustrated in Figs. 16 and 17. Directly beneath it is a load-bearing column, which may induce some differences between the obtained data and the vibration frequencies of the stone statue model. Table 5 presents the comparison of the first three frequencies obtained from environmental stimulation and those from the finite element model for the stone statues. The closely aligned frequency ranges validate the accuracy of the model.

As for the Bodhisattva statues placed on the floor slab, the frequencies obtained from actual measurements are not accurate. As such, to maximize the model's accuracy, efforts should be made during the model development process to align as closely as possible the elastic modulus and other parameters of the model with those of the statutes and ensure that the mechanical laws of the model material meet the current material properties of the stone statues.

Input-time histories

In this study, the incremental dynamic analysis method is employed to subject the model to time history input. The aforementioned vibration test results serve as the basis for the time history curve. Safety Regulations for Blasting Vibration (GB6722-2014) [26] specify an acceptable particle velocity of 1.00 mm/s for general ancient buildings and monuments as the upper limit. After peak amplitude modulation, this value is applied as the excitation for the corresponding working condition and inputted into the model for analysis. According to the existing environmental vibration levels affecting the Buddha statues and the Bodhisattva statues, the peak velocities of the time history curves in each direction were gradually increased based on the Z (vertical) direction velocity in each working condition to obtain the time history curves of different intensities in the different working conditions. The

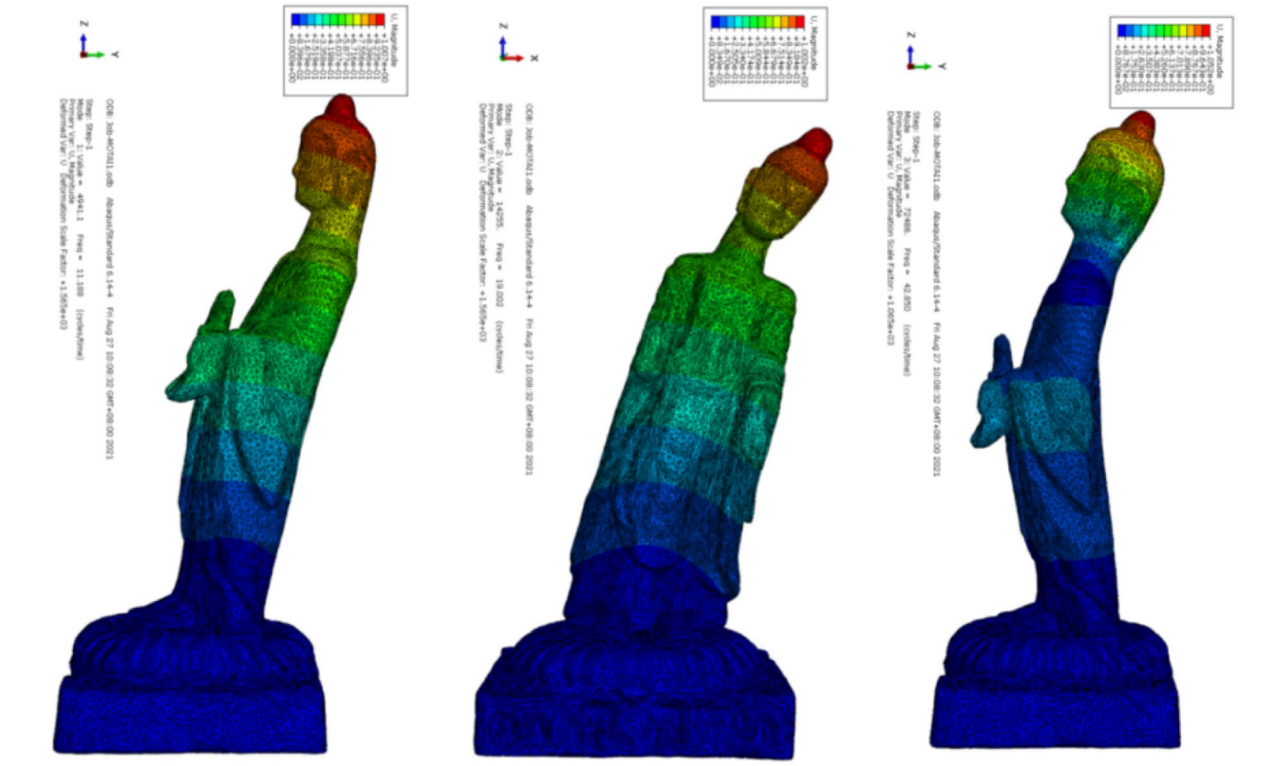

Fig. 14 The first three vibration modes of the left Buddha statue

Z-direction peak velocities of each intensity after amplitude modulation are shown in Tables 6 and 7.

Results and discussion

Vulnerable points at the heads, necks, wrists and feet of the images were selected according to the damage deformation predictions of the model as shown in Figs. 18, 19, 20 and 21, and the predicted maximum tensile stress, maximum strain and maximum shear stress of each point was computed. These are shown in Figs. 22, 23, 24, 25, 26, 27, 28, 29, 30, 31, 32 and 33. In the figures time history 1 corresponds to the Z direction velocity peak of the 1.00 mm/s plastic damage deformation diagram and an output point.

Tensile stress

Figures 22 and 23 show that the maximum tensile stress at each of the measuring point of the two Buddha statues is positively correlated with the overall intensity in the different time histories. Among them, the maximum tensile stress at the foot and neck is larger than elsewhere. The maximum tensile stress in the foot of the right Buddha statue is predicted to be 0.69 MPa under the action of the time history 3 curve, and in the neck 0.34 MPa is predicted. Under the same time history, the overall tensile stress of the right Buddha is greater than that in the left Buddha.

Figures 24 and 25 show similar correlation between the maximum tensile stress and the overall intensity for the two Bodhisattva statues. The maximum tensile stress at the foot and at the front of the neck is relatively large. The maximum tensile stress of the foot of 0.24 MPa is predicted in the Kwanyin Bodhisattva statue under the action of time history 2. The maximum tensile stress in the front of the neck of 0.15 MPa is predicted in the Mahastamaprapta statue under the action of time history 3. For a given time history, the overall tensile stress of the Mahastamaprapta statue is greater than that of the Kwanyin Bodhisattva statue.

Strain

Figures 26 and 27 show that the maximum strain of each measuring point of the two Buddha statues is positively correlated with the overall intensity under different time histories. The maximum strain values at the foot and the neck are relatively large, and those are the weak parts of the statues. The maximum positive strain of 6.52×10^{-5} is predicted at the foot of the right Buddha statue under the action of time history 3. The maximum positive neck strain is 4.67×10^{-5}, which is predicted in the left Buddha

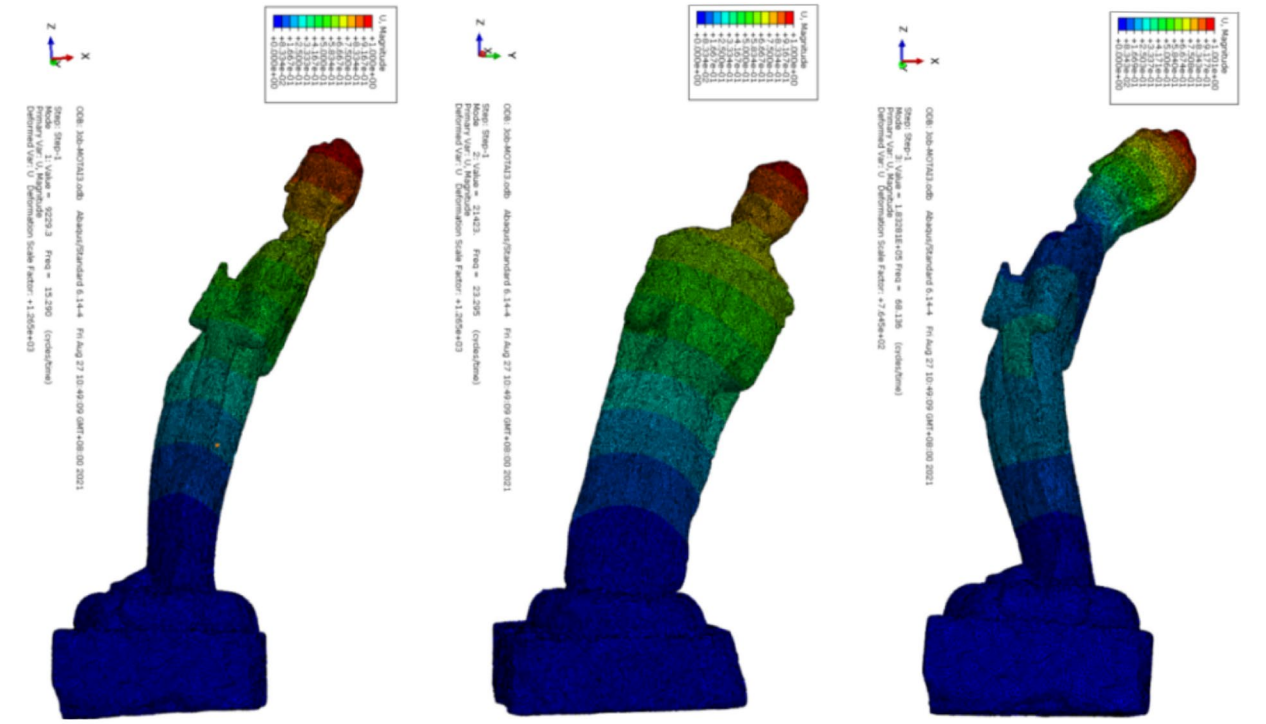

Fig. 15 The first three vibration modes of the Mahastamaprapta statue

Fig.16 Schematic diagram of measuring points of stone Buddha statues

Fig.17 Schematic of measurement point orientation

statue under the action of time history 3. For the same time history, the overall strain in the right Buddha is greater than that in the left Buddha.

For the two Bodhisattva statues Figs. 28 and 29 show that the maximum strain at each measuring point is again positively correlated with the intensity under the different time histories. The maximum strain values at the statues' weakest points, foot and the front of the neck, are again relatively large. The maximum positive strain at the neck is 4.52×10^{-5}, and at the foot it is 2.83×10^{-5}. Both are predicted in the Mahastamaprapta statue under the action of time history 2. For a given

Table 6 Peak velocity in the Z direction at each intensity for the stone Buddha statues (mm/s)

Intensity	1	2	3	4	5	6	7
Stone Buddha statues	0.15	0.22	0.25	0.40	0.60	0.8	1.00

Table 7 Peak velocity in the Z direction at each intensity for the Bodhisattva statues (mm/s)

Intensity	1	2	3	4	5	6	7	8
Bodhisattva statues	0.08	0.10	0.15	0.30	0.50	0.7	0.90	1.00

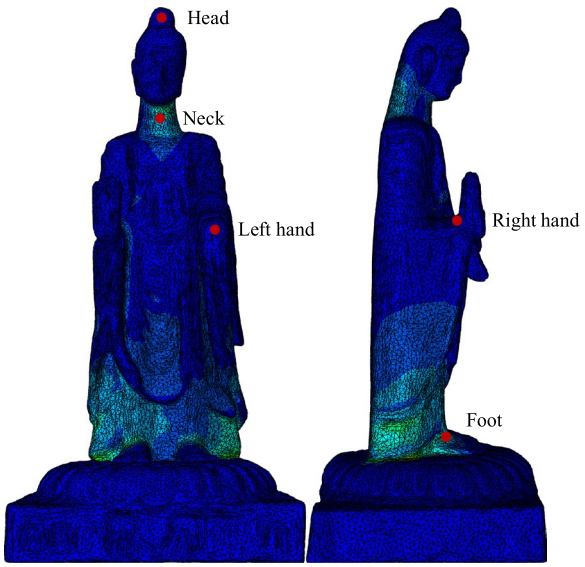

Fig. 18 Diagram of the output point of the left stone Buddha statue

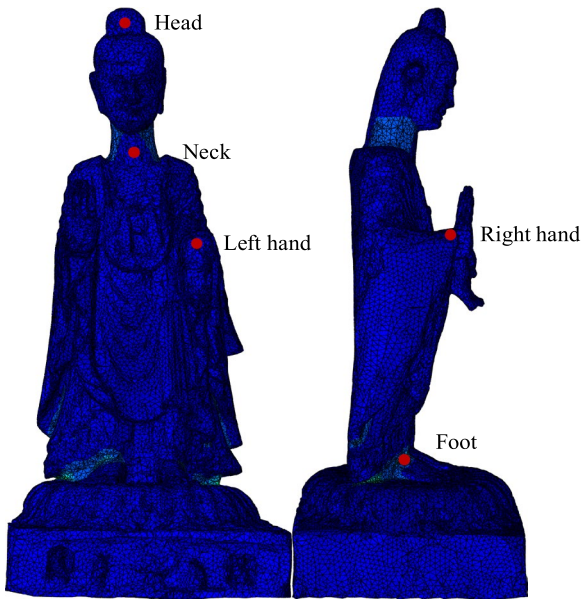

Fig. 19 Diagram of the output point of the right stone Buddha statue

time history, the overall strain in the Mahastamaprapta statue is greater than that in the Kwanyin Bodhisattva.

Shear stress

Figures 30 and 31 show that the maximum shear stress too correlates with the overall intensity for the two Buddha statues under different time histories. The maximum shear stresses are predicted in the right Buddha statue: 0.78 MPa at the foot and 0.36 MPa at its neck, both with time history 3. With each time history the overall shear stress on the right Buddha is stronger than on the left Buddha.

Figures 32 and 33 show the corresponding predictions for the two Bodhisattva statues. The maximum tensile stress at the foot and the front of the neck is relatively strongly correlated with the overall intensity under different time histories. For the Kwanyin Bodhisattva maximum shear stress at the foot is 0.26 MPa, which is produced under the action of time history 1 and the maximum shear stress in the front of the neck is 0.27 MPa under the action of the time history 2. Under the same time history, the overall shear stress on the Kwanyin Bodhisattva statue is greater than that on the Mahastamaprapta statue.

Vibration thresholds

According to the results of numerical simulations, the maximum tensile stress is 0.69 MPa, the maximum strain is 6.52×10^{-5}, and the maximum shear stress is 0.78 MPa. This study adopts a tensile strength threshold of 0.16 MPa for pure water-hardened lime, as indicated in reference [27], for the stone statues. It can be concluded that when stimulated by peak velocities of more than 0.40 mm/s, the maximum tensile stress in the neck and feet of the statues will exceed the tensile strength of the repair material, pure water-hardened lime (0.16 MPa), which constitutes risks of cracking in the repaired areas. In 1984 the Institute of Mechanics of the Chinese

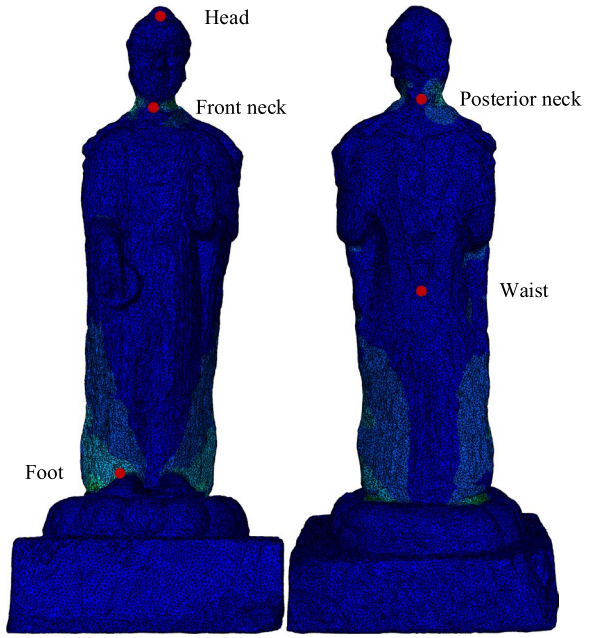

Fig. 20 Schematic diagram of the output point of the statue of Mahasthamaprapta Bodhisattva

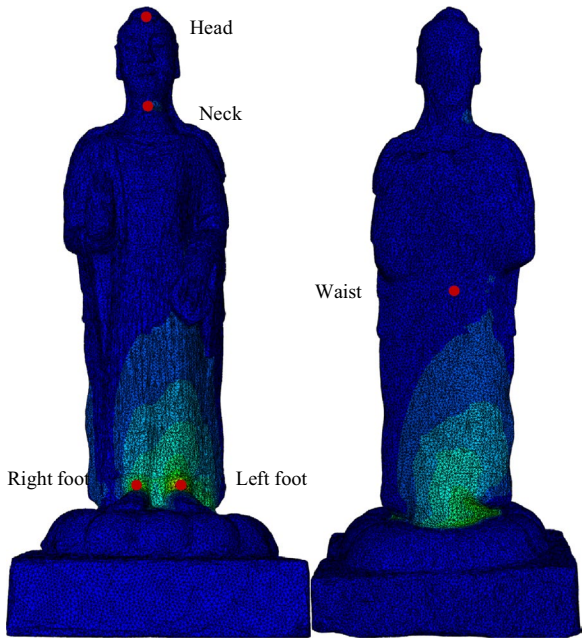

Fig. 21 Schematic diagram of the output point of the statue of Kwanyin Bodhisattva

Academy of Sciences performed bending fatigue tests on Longmen Grottoes rock samples [28] and found a maximum critical strain value of 7.5×10^{-5} for such rock. That is much larger than the maximum strain predicted by the numerical simulations. Table 1 shows that the cohesive force of the limestone is 53 MPa, which is much larger than the maximum shear stress predicted by the numerical simulations. Therefore, without considering other factors, the maximum 1 mm/s vibration considered in the numerical simulations should not cause deformation damage, tensile failure or shear failure in theory, though the maximum tensile stress is close to the critical value of the repair material, which should be considered.

The British Standards Institute considers 0.14 mm/s to be the lowest vibration velocity perceived in most construction-related activities and 0.30 mm/s to be allowable in residential areas [29]. There is guidance available, however, from some similar studies worldwide. When the Metropolitan Museum of Art redecorated its Egyptian galleries, researchers tested the vibrations from the construction equipment to be used on the floors and walls such as levers, hammers, chippers and drills. They found that setting different vibration thresholds for different construction operations in different areas could be an effective control measure. One of their vibration thresholds for heavy equipment was 3.0 mm/s [15]. Vibration tests at the Dutch Museum of Natural History suggest that to ensure the safety of works of art vibration of the floor or shelf should not exceed 1.5–2.0 mm/s during construction work [30]. Johnson reports [15] that many institutions have used 2.54 mm/s as a limit to protect cultural relics in museums from building vibration. in During the construction of buildings surrounding the National Museums in Liverpool, researchers used previous vibration measurements and mathematical statistics to set vibration thresholds between 1.5 and 3.0 mm/s to ensure the safety of easily-damaged paintings and other collections [31].

In contrast to international standards, China's Safety Regulations for Blasting Vibration stipulate particle velocity of 1–2 mm/s for the safety of ancient buildings and monuments. In China, the authoritative specification for this related issue is the Technical Specifications for Protection of Historic Buildings against Man-Made Vibration [32]. Compared to other standards, this specification is more stringent in terms of permissible vibration levels for ancient building structures. It posits that industrial vibrations (such as construction-made vibrations) create a long-term, minimal impact on the structure of ancient buildings; ancient building structures possess non-duplicated historical, cultural, and scientific value compared to their modern counterparts. Based on these two considerations, the specification adopts fatigue limit as the control standard for acceptable vibration standards in ancient building structures to ensure both structural safety (avoiding structural damage) and building safety (preventing minor cracks) for the preservation of the structural integrity of ancient buildings. In accordance

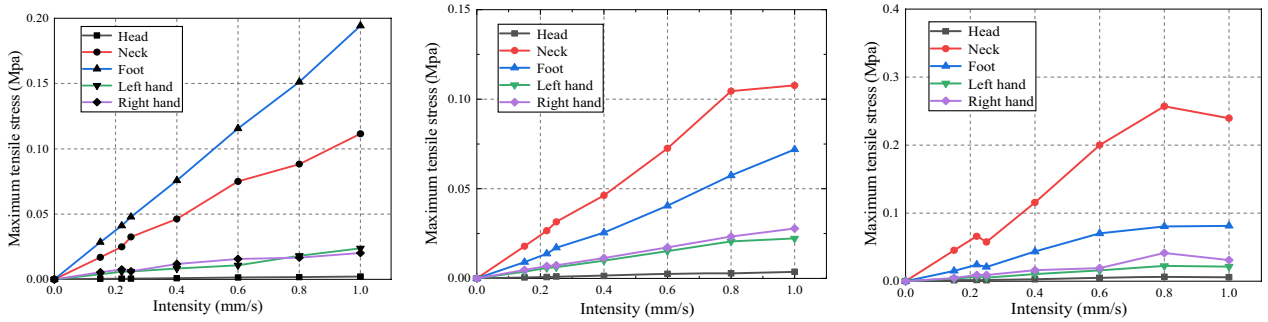

(a) Time history 1 (b) Time history 2 (c) Time history 3

Fig. 22 Relationship between the intensity and maximum tensile stress for the left Buddha

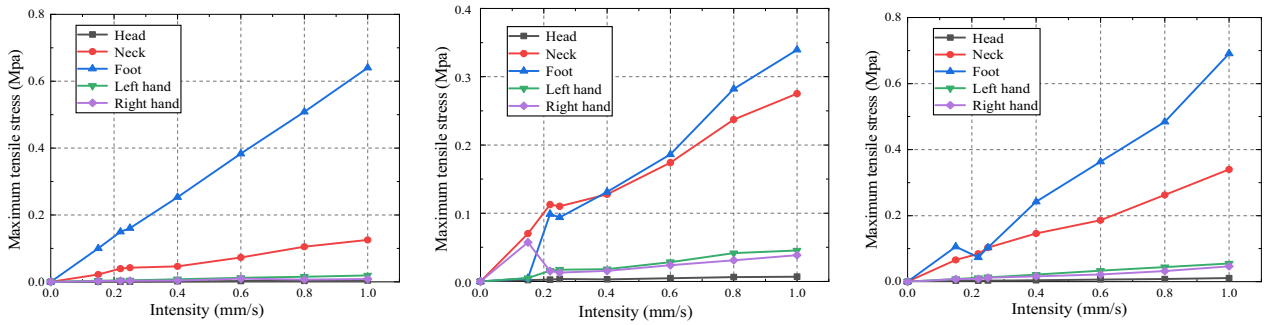

(a) Time history 1 (b)Time history 2 (c) Time history 3

Fig. 23 Relationship between the intensity and maximum tensile stress for the right Buddha

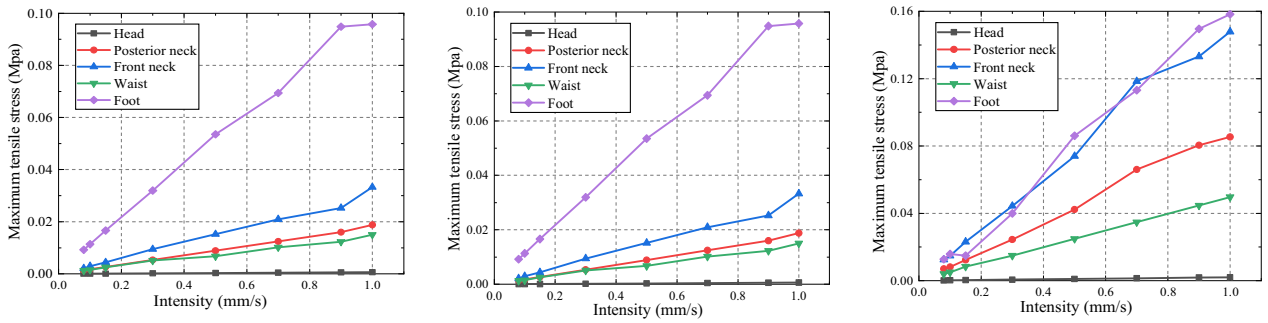

(a) Time history 1 (b) Time history 2 (c) Time history 3

Fig. 24 Relationship between the intensity and maximum tensile stress for the Mahastamaprapta statue

with this specification, the acceptable vibration velocity for stone structures of ancient buildings in the horizontal direction is 0.20 mm/s. Furthermore, Ma et al. [33] discussed the vibration standard classification in this specification and suggested that the control of vibrations in ancient buildings take account of factors such as the previous maintenance and reinforcement of the structure, the current preservation of the cultural relic building, and the recognition of its historical and cultural value. They proposed a matrix applicable to urban ancient buildings: a micro-vibration control matrix. According to the matrix, the vibration velocity limits for nationally designated stone structure buildings range from 0.20 to 0.25 mm/s and from 0.22 to 0.31 mm/s for nationally designated limestone caves.

All four stone sculptures are made of limestone. Specifically, two stone Buddha sculptures have larger dimensions and better integrity, and they are connected

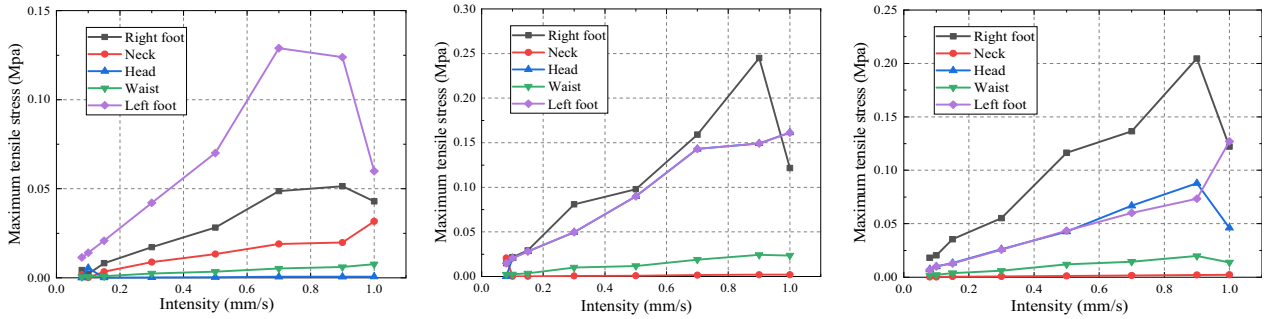

(a) Time history 1 (b) Time history 2 (c) Time history 3

Fig. 25 Relationship between the intensity and maximum tensile stress for the Kwanyin Bodhisattva

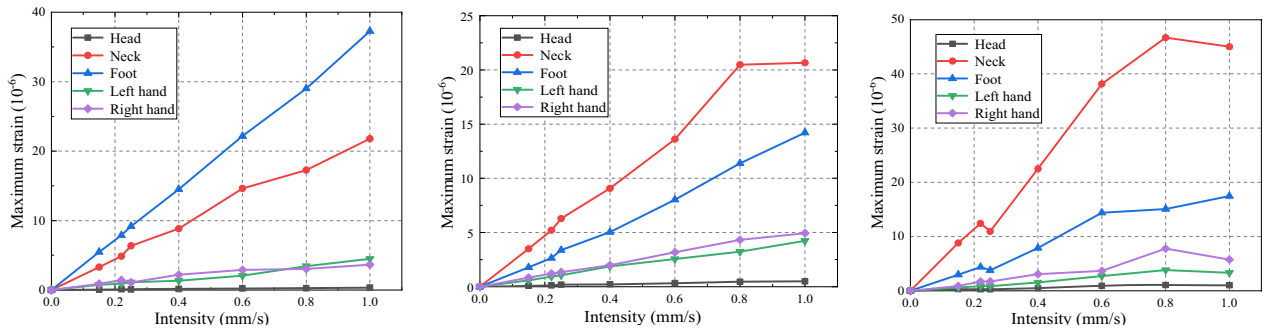

(a) Time history 1 (b) Time history 2 (c) Time history 3

Fig. 26 Relationship between the intensity and maximum strain for the left Buddha

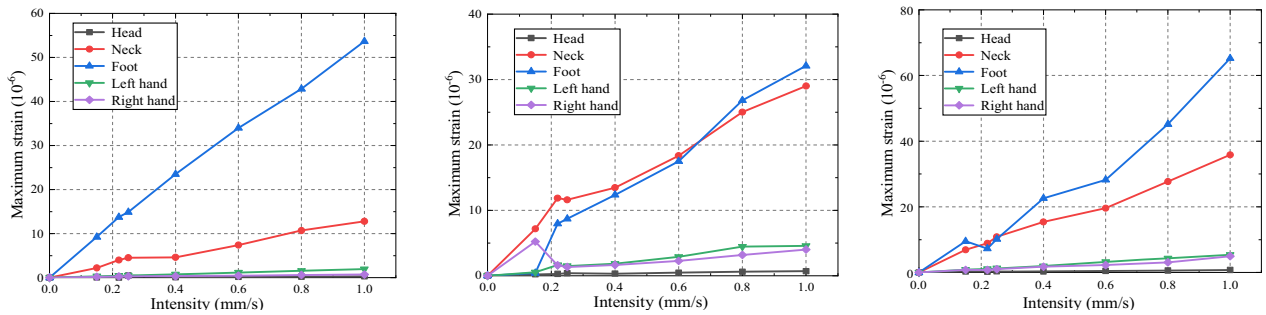

(a) Time history 1 (b) Time history 2 (c) Time history 3

Fig. 27 Relationship between the intensity and maximum strain for the right Buddha

with independent foundations and the ground, ensuring greater stability. The head of the Bodhisattva sculpture, which was restored at a later date, has suffered extensive damage. It is directly supported by the floor slab, resulting in compromised structural integrity and reduced resistance to vibrations. Therefore, the construction vibration protection standard for two Bodhisattva sculptures should be stricter and smaller than that for stone Buddha sculptures. Based on the listed information, the closest protection objects to our research focus are the "Technical Specifications for Protection of Historic Buildings against Man-made Vibration" and "Blasting Safety Regulations". The former protects ancient building stone structures and grottoes with environmental vibration as its vibration property. While the latter protects general ancient buildings and artifacts with construction blasting vibration as its vibration property. They are closer to the

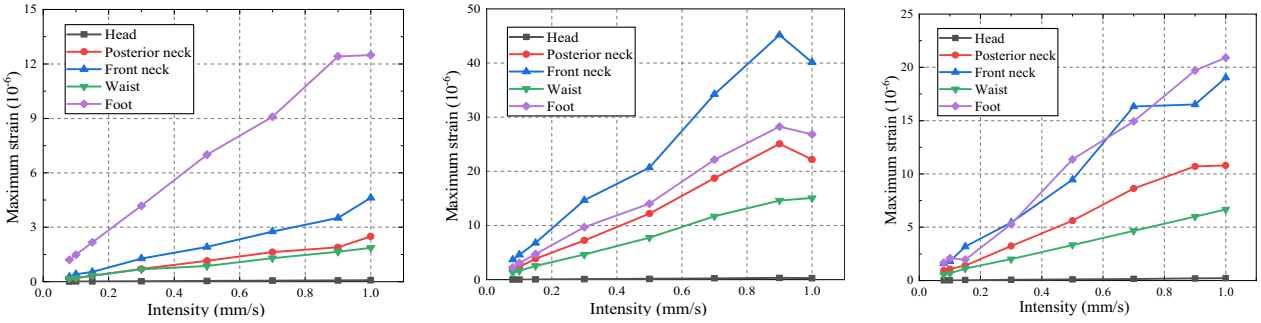

(a) Time history 1 (b) Time history 2 (c) Time history 3

Fig. 28 Relationship between the intensity and maximum strain for the Mahastamaprapta statue

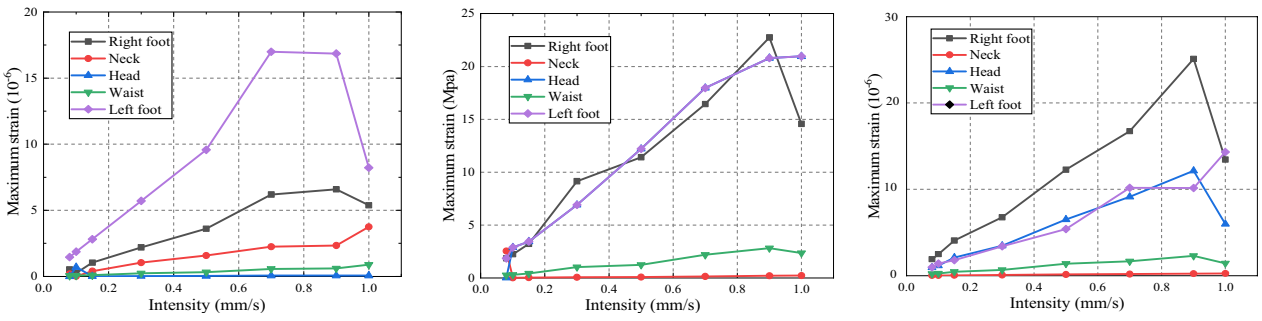

(a) Time history 1 (b) Time history 2 (c) Time history 3

Fig. 29 Relationship between the intensity and maximum strain for the Kwanyin Bodhisattva

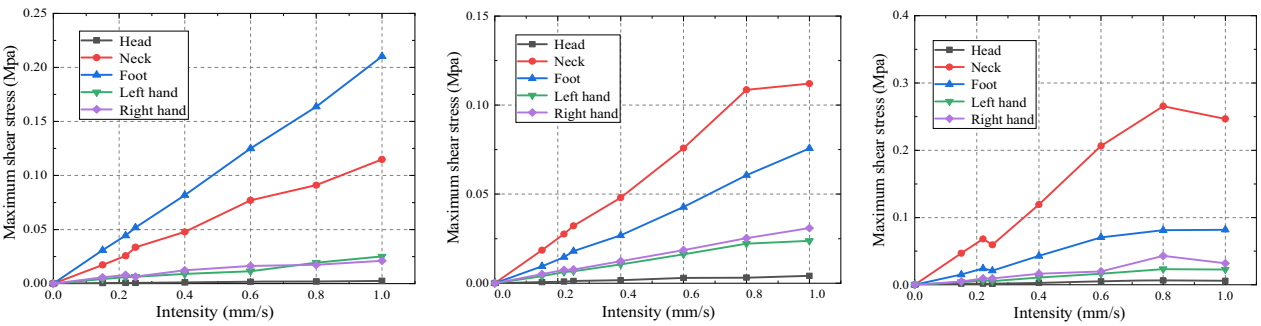

(a) Time history 1 (b) Time history 2 (c) Time history 3

Fig. 30 Relationship between the intensity and maximum shear stress in the left Buddha

protection objects of stone sculptures and construction disturbance. Therefore, the protection standard value can be selected according to the above standards.

Intact statues of this kind would resist peak vibration velocities of 1.0 mm/s without deformation, tension damage or shear damage. However, in view of the actual conditions of these statues, to ensure their safety it is reasonable to use 0.22 to 1.0 mm/s as the reference vibration threshold.

Conclusions

The study delved into the potential impact of vibration from nearby construction on four ancient stone statues in the Qingdao Museum. To achieve this, simulated but full-scale drilling, excavation and impact breaking were conducted to gather ground motion data. The data were then utilized to generate incremental dynamic time histories. Numerical models were developed for the four stone statues and were used for the estimation

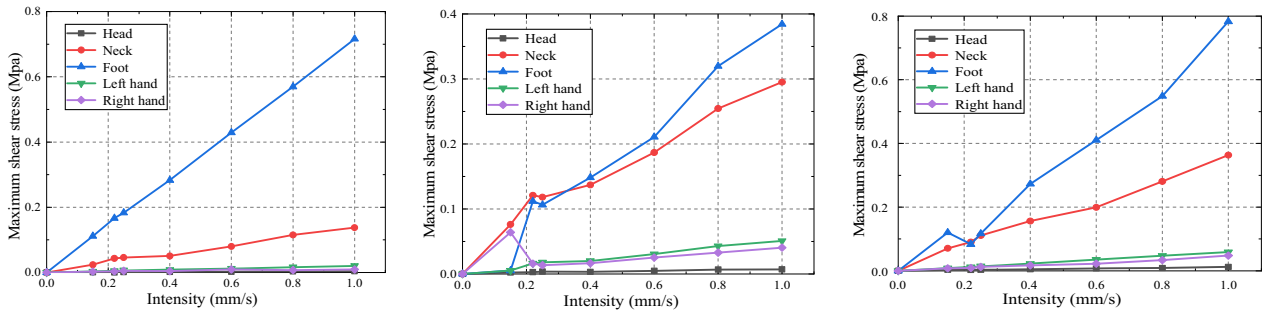

(a) Time history 1 (b) Time history 2 (c) Time history 3

Fig. 31 Relationship between the intensity and maximum shear stress in the right Buddha

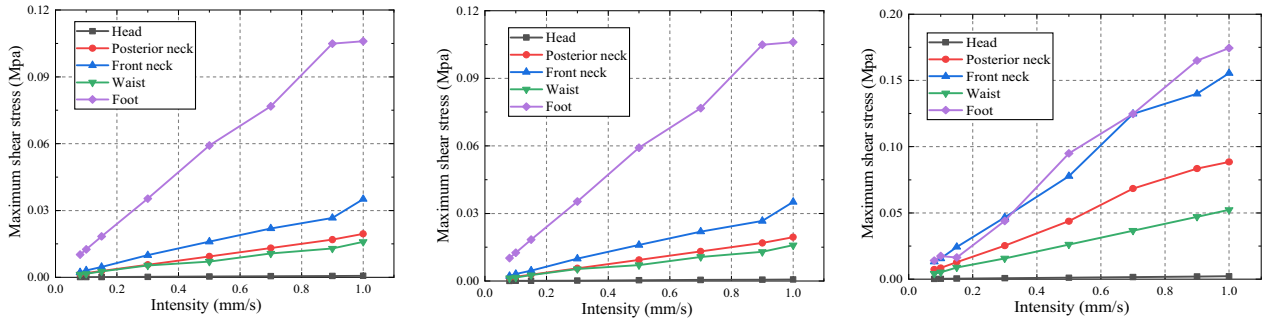

(a) Time history 1 (b) Time history 2 (c) Time history 3

Fig. 32 Relationship between the intensity and maximum shear stress in the Mahastamaprapta statue

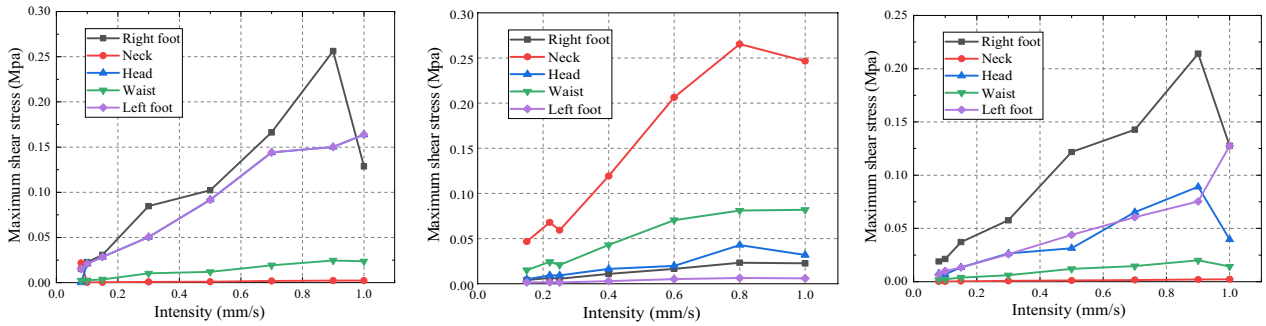

(a) Time history 1 (b) Time history 2 (c) Time history 3

Fig. 33 Relationship between the intensity and maximum shear stress in the Kwanyin Bodhisattva

of various parameters such as maximum tensile stress, maximum strain and maximum shear stress in response to the time histories. This analysis helps identify the most vulnerable parts of the statue, and vibration limits were proposed as a reference for the assessment and protection of similar artifacts from vibration. The main conclusions drawn from this research can be summarized as follows:

1. The numerical simulation shows that the weak positions in all four statues are at the foot and the front of the neck. The numerical modeling technique demonstrated here provides a scientific basis for future construction vibration monitoring and for determining the vulnerable parts of other similar cultural relics.
2. The frequency domain of construction drilling, excavation and impact breaking is approximately

30–50 Hz. All belong to the high-frequency vibration.

3. A reference range for the safe vibration exposure to the four relics has been established. To ensure their safety it is reasonable to use 0.22–1.0 mm/s as the reference vibration threshold.
4. The techniques demonstrated here provide a reliable basis for setting vibration thresholds for engineering construction involving other similar cultural relics.

Acknowledgements
Not applicable.

Author contributions
WX and JZ were responsible for most of the work and writing of the manuscript, WY and DY were responsible for the data analysis of the manuscript, LQ, ZC and YQ have been reviewed and edited the writing of the manuscript. All authors read and approved the final manuscript.

Funding
This research was supported by Natural Science Foundation of Shandong Province (Grants ZR2022ME029 and ZR2020ME246).

Availability of data and materials
All data generated or analyzed during this study are included in the article.

Declarations

Ethics approval and consent to participate
Not applicable.

Consent for publication
Not applicable.

Competing interests
The authors declare that they have no competing interests.

Received: 11 May 2023 Accepted: 20 November 2023
Published online: 30 November 2023

References

1. Bedon C. Experimental investigation on vibration sensitivity of an indoor glass footbridge to walking conditions. J Build Eng. 2020;29:01195. https://doi.org/10.1016/j.jobe.2020.101195.
2. Van Nimmen K, Lombaert G, De Roeck G. The impact of vertical human–structure interaction on the response of footbridges to pedestrian excitation. J Sound Vib. 2017;402:104–21. https://doi.org/10.1016/j.jsv.2017.05.017.
3. Azzara RM, Girardi M, Iafolla V, Lucchesi DM, Padovani C, Pellegrini D. Ambient vibrations of age-old masonry towers: results of long-term dynamic monitoring in the historic centre of Lucca. INT J ARCHIT HERIT. 2021;15(1):5–12. https://doi.org/10.1080/15583058.2019.1695155.
4. Negreira J, Trollé A, Jarnerö K, Sjökvist LG, Bard D. Psycho-vibratory evaluation of timber floors: towards the determination of design indicators of vibration acceptability and vibration annoyance. J Sound Vib. 2015;340:383–408. https://doi.org/10.1016/j.jsv.2014.12.001.
5. Brennan MJ, Tang B, Melo GP, Lopes V. An investigation into the simultaneous use of a resonator as an energy harvester and a vibration absorber. J Sound Vib. 2014;333(5):1331–43. https://doi.org/10.1016/j.jsv.2013.10.035.
6. Gordon CG. Generic criteria for vibration-sensitive equipment. Vib Control Microelectron Opt Metrol. 1992;1619:75–81. https://doi.org/10.1117/12.56826.
7. Wei W, Sauvage L, Wölk J. Baseline limits for allowable vibrations for objects. Prevent Conserv. 2014;1516:7.
8. Nicoletti V, Quarchioni S, Tentella L, Martini R, Gara F. Experimental tests and numerical analyses for the dynamic characterization of a steel and wooden cable-stayed footbridge. Infrastructures. 2023;8(6):100. https://doi.org/10.1016/j.jobe.2021.103764.
9. Nicoletti V, Arezzo D, Carbonair S, Gara F. Detection of infill wall damage due to earthquakes from vibration data. Earthq Eng Struct Dyn. 2023;52(2):460–81. https://doi.org/10.1002/eqe.3768.
10. Nicoletti V, Arezzo D, Carbonari C, Gara F. Dynamic monitoring of buildings as a diagnostic tool during construction phases. J Build. 2022;46:103764. https://doi.org/10.1016/j.jobe.2021.103764.
11. Kracht K, Kletschkowski T. From art to engineering, a technical review on the problem of vibrating canvas part I: excitation and efforts of vibration reduction. Mech Eng. 2017;15(1):163–82. https://doi.org/10.22190/FUME161010009K.
12. Johnson AP, Hannen WR. Vibration limits for historic buildings and art collections. APT Bull J Preservat Technol. 2015;46(2/3):66–74.
13. Stefano A, Clemente P. Structural health monitoring of historical structures. In: Structural health monitoring of historical structures. Cambridge: Woodhead Publishing; 2009. p. 412–34. https://doi.org/10.1533/9781845696825.2.412.
14. Johnson AP, Hannen WR, Zuccari F. Vibration control during museum construction projects. J Am Inst Conserv. 2013;52(1):30–47. https://doi.org/10.1179/0197136012Z.0000000003.
15. Johnson A, El Batanouny M, Simpsonn W. Vibration mitigation and sound testing in SUE Hall at the Field Museum in Chicago. APT Bull J Preservat Technol. 2020;51(4):45–50. https://www.jstor.org/stable/26970192.
16. Okumus P, Oliva MG, Hoehn T. Impact of cast-in-place concrete column construction vibrations on sensitive occupancies. Pract Period Struct Des Constr. 2015;20(1):04014023. https://doi.org/10.1061/(ASCE)SC.1943-5576.0000220.
17. Zini G, Betti M, Bartoli G. Experimental analysis of the traffic-induced vibration on an ancient lodge. Struct Control Health. 2021;29(3):e2900. https://doi.org/10.1002/stc.2900.
18. Pieraccini M, Betti M, Forcellini D, Dei D, Papi F, Bartoli G, et al. Radar detection of pedestrian-induced vibrations on Michelangelo's David. PLoS ONE. 2017;12(4):e0174480. https://doi.org/10.1371/journal.pone.0174480.
19. Siami A, Cigada A, Zappa E. Vibration protection of cultural heritage objects. In: Vibration control and actuation of large-scale systems. San Diego: Academic Press; 2020. p. 107–56. https://doi.org/10.1016/B978-0-12-821194-6.00005-6.
20. Dai YJ, Liu T. Study on protection technology of metro shield tunneling under-passing vibration hypersensitive building. Commun Sci Technol Heilongjiang. 2019;42(10):139–42. https://doi.org/10.16402/j.cnki.issn1008-3383.2019.10.067. (**in Chinese**).
21. Fu CH, Shi YC, Qiu RD. Numerical simulation of the mechanism of seismic deformation and damage of country rock of the Longmen grottoes. J Seismol Res. 2011;34(2):194–200, 254 (**in Chinese**).
22. Fjær E, Holt RM, Horsrud P, Raaen AM, Risnes R. Elastic wave propagation in rocks. Dev Pet Sci. 2008;53:175–218. https://doi.org/10.1016/S0376-7361(07)53005-0.
23. Rukhaiyar S, Samadhiya NK. Triaxial strength behaviour of rockmass satisfying modified Mohr–Coulomb and generalized Hoek–Brown criteria. Int J Min Sci Technol. 2018;28(6):901–15. https://doi.org/10.1016/j.ijmst.2017.11.004.
24. Menetrey P, Willam KJ. Triaxial failure criterion for concrete and its generalization. Struct J. 1995;92(3):311–8.
25. Kong WX, Rui YQ, Dong BD. Determination of dilatancy angle for geomaterials under non-associated flow rule. Rock Soil Mech. 2009;30(11):3278–82 (**in Chinese**).
26. Administration CNS. GB 6722–2014-safety regulations for blasting. Beijing: Standards Press of China; 2014. (**in Chinese**).
27. Li Y, Yu PC, Liu JP, Li H. Preparation and durability of modified hydraulic lime-based material. J Beijing Univ Technol. 2017;43(2):269–77 (**in Chinese**).
28. Zhang CY. The analysis of rock mass fatigue effects under vibration environment in Luoyang Longmen grottoes. Acta Scientiarum Naturalium Universitatis Pekinensis. 2002;38(6):809–16. https://doi.org/10.13209/j.0479-8023.2002.141. (**in Chinese**).

29. British Standards Institution. BS 5228-2:2009-code of practice for noise and vibration control on construction and open sites part 2: vibration. London: British Standards Institution; 2009.
30. Wei W, Dondorp E. Testing to determine allowable vibration limits at a natural-history museum in The Netherlands. APT Bull J Preservat Technol. 2020;51(4):19–26. https://www.jstor.org/stable/26970189.
31. Wei W, Watts S, Seddon T, Crombie D. Protecting museum collections from vibrations due to construction: vibration statistics, limits, flexibility and cooperation. Stud Conserv. 2018;63(Supp 1):293–300. https://doi.org/10.1080/00393630.2018.1504438.
32. Ministry of Housing and Urban-Rural Development of the People's Republic of China. GB/T 50452-2008-Technical specifications for protection of historic buildings against man-made vibration. Beijing: China Architecture & Building Press; 2008 (**in Chinese**).
33. Ma M, Liu WN, Zheng SL, Sun X. Discussion of vibration classification for historic buildings. Sci Conserv Archaeol. 2013;25(1):54–60. https://doi.org/10.16334/j.cnki.cn31-1652/k.2013.01.008. (**in Chinese**).

Publisher's Note